Towards High-Data-Rate Noncoherent Chaotic Communication: A Multiple-Mode Differential Chaos Shift Keying System

Xiangming Cai,   Weikai Xu, *Member, IEEE,* Lin Wang, *Senior Member, IEEE,*   Guanrong Chen, *Life Fellow, IEEE*

Abstract—In this paper, we focus on designing a high-data-rate noncoherent chaotic communication scheme to satisfy the demand of the explosive growth in data traffic. To achieve this goal, a joint time-frequency index modulation assisted multiple-mode DCSK (JTFIM-MM-DCSK) system is proposed, where a pair of distinguished signal modes are modulated into the selected subcarriers and another signal mode is transmitted by the unselected subcarriers. In this configuration, besides the modulated bits used for physical transmission, the carrier index bits and time slot index bits, conveyed by the state of whether subcarriers and time slots are selected or not, are also transmitted implicitly to achieve higher data rate. Moreover, the design of multiple-mode signals ensures that it is taking full advantage of all subcarriers and time slots to transmit the information bits, thereby improving the data rate significantly. The bit error rate (BER) expressions of the JTFIM-MM-DCSK system are derived over additive white Gaussian noise (AWGN) and multi-path Rayleigh fading channels, which are checked by computer simulations. Finally, the advantage of the JTFIM-MM-DCSK system over other up-to-date noncoherent chaotic communication systems is demonstrated in terms of BER performance through extensive computer simulations.

Index Terms—Noncoherent chaotic communication, differential chaos shift keying (DCSK), time-frequency index modulation, multiple-mode signal design, high-data-rate transmission.

I. INTRODUCTION

With a great potential to offer many favorable advantages, such as easy generation even by a simple nonlinear circuit with very few off-the-shelf electronic components, a delta-function-like auto-correlation property, wide-band, non-periodic and random-like features, chaotic signals have been recognized as the excellent candidate for spread-spectrum communication (SS) and secure communication [1]. Chaotic communication utilizing the chaotic signal as its carrier has been the subject of continued interest in the last two decades [2]. Generally, chaotic communication can be categorized as coherent and noncoherent schemes according to whether the exact replicas of the unmodulated chaotic carriers are needed at the receiver [3]. As a typical representative of coherent chaotic communication schemes, the chaos shift keying (CSK) system [4], [5]

can provide better robustness in contrast to the noncoherent counterparts. Unfortunately, these coherent schemes are restricted by the complicated and difficult chaos synchronization. Although increasing efforts have been devoted to studying synchronization algorithms [6]–[8], very little progress was made in tackling this obstacle.

A low-complexity noncoherent differential chaos shift keying (DCSK) system [9], [10] is configured with a simple auto-correlation receiver (AcR), where the structure of the transmitted-reference (TR) signal can avoid the requirement of chaos synchronization. DCSK system, which involves the transmission of a reference and data signal pair separated in the time domain, is capable of exploiting the multipath diversity inherently to achieve good BER performance in the diffuse environment without the need for channel state information (CSI) and channel estimation [11]–[13]. Nevertheless, the introduction of TR configuration in the DCSK system lowers the data rate, because half of the symbol duration is applied to transmit the non-data-carrying reference signal. Specifically, the reference chaotic signal is arranged in the first time slot, and the second time slot will carry either the reference signal itself or a negated version depending upon the symbol being sent. Since the advent of the next generation wireless networks would give rise to an explosive growth in data traffic, there is a compelling interest in studying and designing high-data-rate communication systems.

A feasible way to achieve the goal of high-data-rate chaotic communication is an integration of M-ary modulation with the DCSK system, which had resulted in the well-known quadrature chaos shift keying (QCSK) [14], M-ary DCSK [15] and square-constellation-based M-DCSK [16] schemes. Another alternative approach to increasing the data rate of the DCSK system is to transmit more than one information-bearing signal after the reference signal [17], in which the data rate and energy efficiency are improved by sharing the same reference signal. In [18] and [19], a signal design for the DCSK system is implemented to double the data rate and improve the system security. In addition, the improved DCSK (I-DCSK) [20] system applies a time-reversal operation in its signal design, making the reference signal orthogonal to the data carrier signal so as to allow summation, thus providing the double data rate. In [21], by shortening the proportion of reference signal relative to the overall transmitted symbol duration, a short reference DCSK (SR-DCSK) system was proposed to increase the data rate and improve the energy
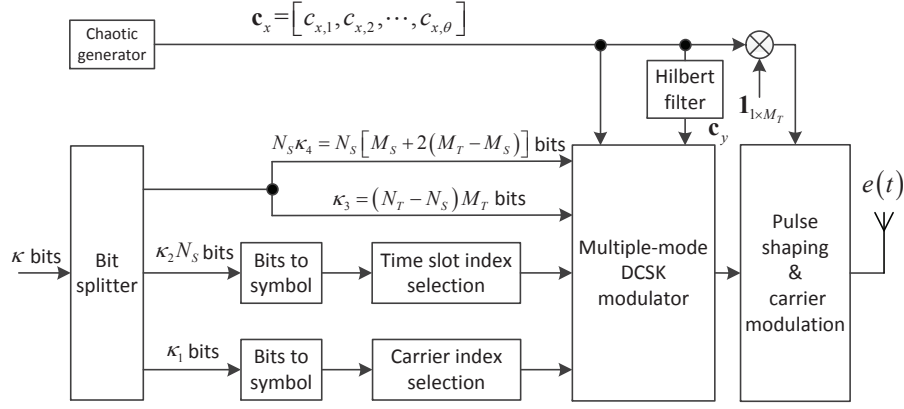
Fig. 1.   Block diagram of the JTFIM-MM-DCSK transmitter.

efficiency without penalizing the BER performance.

Based on orthogonal Walsh codes, a code-shifted DCSK (CS-DCSK) system with a delay-line-free receiver was proposed in [22], where the reference and information-bearing signals are overlapped in the same time slots. Following this work, a generalized CS-DCSK (GCS-DCSK) system integrates the reference and multiple information-bearing signals into the same symbol period in a superimposed manner, thereby providing higher data rate [23]. However, the BER performance of the GCS-DCSK system is deteriorated with the increasing number of parallel information-bearing signals. In this regard, a multilevel coded-shifted M-ary DCSK (MCS-MDCSK) system [24] was proposed to harvest the benefits of multilevel M-ary modulation in terms of high data rate avoiding a downgrade of BER performance. Moreover, to break the restriction of the limited number of Walsh codes, the CS-DCSK system was extended to a high-data-rate CS-DCSK (HCS-DCSK) system [25] via replacing the Walsh codes by orthogonal chaotic sequences. An orthogonal multilevel DCSK (OM-DCSK) system [26] was capable of achieving high-data-rate transmission by constructing an ample orthogonal signal set. More recently, enjoying the advantages of the discrete-cosine-spreading (DCS) codes, a high-data-rate DCS-MDCSK system was proposed in [27] to obtain a high data rate with a low peak-to-average-power ratio (PAPR).

In response to the increasing demand for high-data-rate communications fueled by the continuing growth of smart devices and mobile applications, the next-generation wireless communications systems are actively exploring key techniques to provide high-data-rate communication services [28]. Index modulation (IM) has been recognized as a novel technique to accommodate the demand of high-data-rate transmission [29]. In IM configuration, only a fraction of certain indexed entities, e.g., antennas, spreading codes, subcarriers, time slots and so forth, are activated for information transmission, while the others leave unused [30]. In this process, additional information bits are transmitted by the index symbols in an implicit manner. Due to these advantages, the IM paradigm was applied to DCSK-based systems, such as CS-DCSK and OM-DCSK, and two kinds of code index modulation assisted DCSK systems (named CIM-CS-DCSK [31] and CIM-OM-

MDCSK [32], respectively) were developed to obtain higher data rates. Furthermore, encouraged by the benefits of the IM technique, the permutation index DCSK (PI-DCSK) [33] and commutation code index DCSK (CCI-DCSK) [34] systems were proposed, where the extra information bits are conveyed by the indices of permuted or commutated replicas of the reference signal.

Recently, the iterative chaotically shift-aided shuffling and overlapping operations were applied in the overlapping chaotic chip position shift keying (OCCPSK) [35] system to enhance system security. Different from the multiuser orthogonal frequency division multiplexing (OFDM) based DCSK (MU-OFDM-DCSK) [36] system, a frequency-hopping OFDM-DCSK (FH-OFDM-DCSK) [37] system fully exploits the frequency and time diversity to improve system reliability. In [38], a chaotic shape-forming filter assisted M-ary DCSK (CSF-M-DCSK) system was proposed, where a coherent matched filter receiver and maximum likelihood decision criterion are used to obtain better BER performance. A carrier interferometry (CI) code aided OFDM-DCSK (CI-OFDM-DCSK) system was proposed in [39] to reduce high PAPR. In addition, a parallel concatenated index modulation based OFDM-DCSK system was proposed in [40], which uses the indices of the rotated carrier interferometry codes to transmit the additional mapped bits, therefore improving the data rate and energy efficiency. Motivated by the position pulse modulation-aided DCSK (PPM-DCSK) [41] system, a low-complexity superposition coding PPM-DCSK (SC-PPM-DCSK) scheme was proposed in [42] to meet the demand of multiuser simultaneous information for systems in the downlink scenario. In order to support continuous-mobility settings, a continuous-mobility DCSK (CM-DCSK) system was developed in [43] to modify the frame structure of the conventional DCSK system, i.e., each reference sample of the CM-DCSK system is followed by a data carrier sample.

Aiming to further increase the data rate of the PPM-DCSK system, a dual-mode DCSK solution based on the IM technique (referred to as DM-DCSK-IM [44]) was proposed, in which the active and inactive time slots were used to carry the distinguishable DCSK and QCSK signals, respectively. Moreover, the IM was introduced into the multicarrier DCSK (MC-

DCSK) system [45] so that the proposed carrier index DCSK (CI-DCSK) [46], its generalized version (GCI-DCSK) [47] and the M-ary scheme (CI-MDCSK) [48] were able to enhance the data rate of the MC-DCSK system. Afterwards, a code index modulation-aided multicarrier M-ary DCSK (CIM-MC-MDCSK) system was proposed in [49] to achieve a higher data rate than the CI-MDCSK system. Since the aforementioned IM-based DCSK systems possess only one dimension (such as time slots, spreading codes or subcarriers) for conveying the additional information bits, there is still enormous room for optimization and enhancement. In addition, IM-based schemes have the ability to transfer the saved transmission energy from the inactive components to the active ones, benefiting the BER performance significantly [29]. Therefore, the indices of multiple dimensions can be integrated together for better BER performance. More importantly, in the exiting DCSK-based systems, a transmitted symbol can only carry relatively few information bits, which can not meet the demand of the explosive growth in data traffic. Although MC-DCSK and OFDM-based DCSK systems can enhance the data rate by multicarrier transmission, the BER performances of these systems are not satisfactory, which restricts the applications of these systems. Given this background, a joint time-frequency index modulation aided multiple-mode DCSK (JTFIM-MM-DCSK) system is designed here to achieve both high-data-rate transmission and better BER performance. The main contributions of this paper are summarized as follows.

1) A joint time-frequency index modulation assisted multiple-mode DCSK system is proposed, where the selected subcarriers are used to modulate a pair of distinguished modem-mode constellations, while the remaining unselected subcarriers are assigned to transmit a signal in another mode. In this case, all subcarriers and time slots are sufficiently exploited to convey the multiple-mode signal in the JTFIM-MM-DCSK system, thereby improving the data rate significantly.

2) The data rate, energy efficiency, spectral efficiency and system complexity of the JTFIM-MM-DCSK system are analyzed and compared to that of other chaotic communication systems. The results show that the proposed JTFIM-MM-DCSK system is capable of obtaining higher data rate, energy efficiency and spectral efficiency at the expense of system complexity.

3) The analytical BER expressions of the JTFIM-MM-DCSK system over AWGN and multipath Rayleigh fading channels are derived and verified by computer simulations. In addition, the superiority of the BER performance of the JTFIM-MM-DCSK system is confirmed by extensive comparisons. It is shown that the JTFIM-MM-DCSK system can obtain 2 to 5dB performance gain over other chaotic communication systems.

The rest of this paper is structured as follows. It begins with the system model description in Section II. The data rate, energy efficiency, spectral efficiency and system complexity of the JTFIM-MM-DCSK system are analyzed in Section III. Section IV provides the theoretical BER expressions for the JTFIM-MM-DCSK system over AWGN and multipath
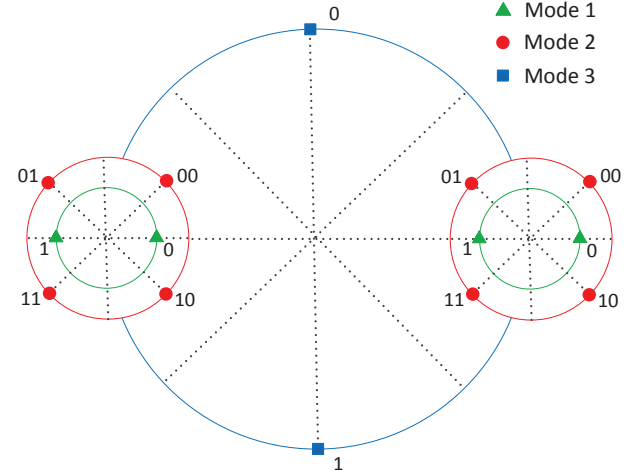

Fig. 2.   Constellation design for multiple-mode DCSK. Mode 1 and 2 denote the signals in the forms of $d_i\mathbf{c}_x$ and $a_i\mathbf{c}_x+b_i\mathbf{c}_y$, respectively, carried by the selected subcarriers. The signal $q_i\mathbf{c}_y$ carried by the unselected subcarriers is corresponding to mode 3.

Rayleigh fading channels. The simulation results are presented in Section V. Finally, Section VI presents some concluding remarks.

II. THE JTFIM-MM-DCSK SYSTEM

A. The Transmitter

The block diagram of the JTFIM-MM-DCSK transmitter is shown in Fig. 1. In the proposed system, N_S out of N_T subcarriers are selected to convey two kinds of distinguishable signals, i.e., $d_i\mathbf{c}_x$ and $a_i\mathbf{c}_x+b_i\mathbf{c}_y$, while the remaining $N_T - N_S$ subcarriers are assigned to transmit the signal $q_i\mathbf{c}_y$. Here, $\mathbf{c}_x = [c_{x,1}, c_{x,2}, \cdots, c_{x,\theta}]$ is a θ-length chaotic signal and $\mathbf{c}_y$, produced by the Hilbert filter, is orthogonal to $\mathbf{c}_x$. In addition, $d_i \in \frac{1}{2}(-1,1)$, $a_i + jb_i \in \frac{\sqrt{2}}{2}(1+j, -1+j, -1-j, 1-j)$ and $q_i \in \frac{1}{2}(-1,1)$ denote the information symbols carried by the corresponding signals of mode 1, 2 and 3, respectively. Fig. 2 shows a constellation design of the multiple-mode DCSK system. Considering a selected subcarrier, M_S out of M_T time slots are chosen to carry the signal $d_i\mathbf{c}_x$ corresponding to mode 1, while the rest time slots are arranged to transmit the signal $a_i\mathbf{c}_x + b_i\mathbf{c}_y$ corresponding to mode 2. Based on the unselected subcarriers, all time slots are used to convey the signal of mode 3, namely $q_i\mathbf{c}_y$.

Since there are N_S subcarriers chosen from N_T subcarriers, the total number of carrier index bits is calculated as $\kappa_1 = \lfloor \log_2 \binom{N_T}{N_S} \rfloor$, where $\binom{\cdot}{\cdot}$ is the binomial coefficient and $\lfloor \cdot \rfloor$ denotes the floor function. In a selected subcarrier, M_S out of M_T time slots are used to convey signal mode 1 and thus the number of time slot index bits equals $\kappa_2 = \lfloor \log_2 \binom{M_T}{M_S} \rfloor$. Consequently, $N_S\kappa_2$ time slot index bits are transmitted by the N_S selected subcarriers. Taking the modulated bits into consideration, the total number of modulated bits carried by the unselected subcarriers is $\kappa_3 = (N_T - N_S)M_T$, while the total number of modulated bits transmitted by a selected subcarrier is $\kappa_4 = M_S + 2(M_T - M_S)$. All subcarriers and time slots are sufficiently utilized to transmit the information

bits, and therefore the number of transmitted bits per JTFIM-MM-DCSK symbol equals

$$
\begin{aligned}
\kappa =& \kappa_1 + N_S\kappa_2 + \kappa_3 + N_S\kappa_4 \\
=& \lfloor \log_2 \binom{N_T}{N_S} \rfloor + N_S \lfloor \log_2 \binom{M_T}{M_S} \rfloor + (N_T - N_S)M_T \\
& + N_S[M_S + 2(M_T - M_S)].
\end{aligned} \tag{1}
$$

The combinational method developed in [50] provides a one-to-one mapping between the index bits and the indices of the selected entities (e.g., subcarriers and time slots). Particularly, according to [50], for fixed n and k ($n > k$), all $Z \in \{0, \binom{n}{k} - 1\}$ can be presented by a strictly decreasing k-length sequence $J_\alpha = \{\alpha_k, \cdots, \alpha_1\}$, $\alpha_k > \cdots > \alpha_1 \geq 0$, which takes elements from the set $\{0, \cdots, n-1\}$ according to the following equation:

$$
Z = \binom{\alpha_k}{k} + \cdots + \binom{\alpha_2}{2} + \binom{\alpha_1}{1}. \tag{2}
$$

As an example, when $n = 6$, $k = 3$ and $\binom{6}{3} = 20$, all elements of J_α can be calculated as

$$
\begin{aligned}
19 &= \binom{5}{3} + \binom{4}{2} + \binom{3}{1} \rightarrow J_\alpha = \{5, 4, 3\} \\
18 &= \binom{5}{3} + \binom{4}{2} + \binom{2}{1} \rightarrow J_\alpha = \{5, 4, 2\} \\
&\vdots \\
10 &= \binom{5}{3} + \binom{1}{2} + \binom{0}{1} \rightarrow J_\alpha = \{5, 1, 0\} \\
9 &= \binom{4}{3} + \binom{3}{2} + \binom{2}{1} \rightarrow J_\alpha = \{4, 3, 2\} \\
&\vdots \\
1 &= \binom{3}{3} + \binom{1}{2} + \binom{0}{1} \rightarrow J_\alpha = \{3, 1, 0\} \\
0 &= \binom{2}{3} + \binom{1}{2} + \binom{0}{1} \rightarrow J_\alpha = \{2, 1, 0\}.
\end{aligned}
$$

The above-mentioned combinational method can be adopted to determine the selected subcarriers and time slots. In other words, carrier index bits are first converted into a decimal number, and then this decimal number is used with the combinational method to obtain the specific carrier indices as $J_\alpha + 1$. Similar operations are performed to obtain the specific indices of the selected time slots. Fig. 3 depicts an example of signal format for the information-bearing signal of the JTFIM-MM-DCSK system.

Define the subcarrier index vector as $\mathbf{v}_s = [v_s(1), v_s(2), \cdots, v_s(i), \cdots, v_s(N_T)]$, in which $v_s(i)$ is either "0" or "1" representing that the ith subcarrier is unselected or selected, respectively. In addition, the time slot index vector within the ith selected subcarrier is defined as $\mathbf{v}_{t,i} = [v_{t,i}(1), v_{t,i}(2), \cdots, v_{t,i}(j), \cdots, v_{t,i}(M_T)]$, in which $v_{t,i}(j) = 0$ means the jth unselected time slot, while $v_{t,i}(j) = 1$ means the jth selected time slot. The transmitted signal within the kth selected subcarriers is expressed as

$$
\mathbf{U}_k = [\mathbf{u}_k(1), \mathbf{u}_k(2), \cdots, \mathbf{u}_k(j), \cdots, \mathbf{u}_k(M_T)], \tag{3}
$$

where $\mathbf{u}_k(j) = \begin{cases} d_{k,j}\mathbf{c}_x, & v_{t,k}(j)=1 \\ a_{k,j}\mathbf{c}_x + b_{k,j}\mathbf{c}_y, & v_{t,k}(j)=0 \end{cases}$. In addition, the signal within the kth unselected subcarriers is given as

$$
\mathbf{W}_k = [\mathbf{w}_k(1), \mathbf{w}_k(2), \cdots, \mathbf{w}_k(j), \cdots, \mathbf{w}_k(M_T)], \tag{4}
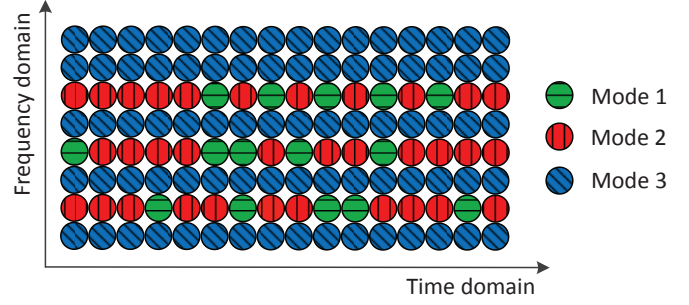$$

Fig. 3. The signal format of the information-bearing signal for the JTFIM-MM-DCSK system, where $N_T = 8$, $N_S = 3$, $M_T = 16$ and $M_S = 5$. When the carrier index bits are $\{0,1,1,1,0\}$, the specific indices of the selected subcarrier are $\{6,4,2\}$. When the time slot index bits corresponding to the selected subcarriers are $\{1,0,0,1,0,0,0,0,1,0,1,0\}$, $\{0,0,1,0,0,0,1,1,0,0,1,0\}$ and $\{0,1,1,0,1,0,1,0,1,1,1,1,1,1,1\}$, the indices of the selected time slots within the selected subcarriers are $\{15,11,10,7,4\}$, $\{12,9,7,6,1\}$ and $\{14,12,10,8,6\}$, respectively.

where $\mathbf{w}_k(j) = q_{k,j}\mathbf{c}_y$. As a result, the overall transmitted signal of the JTFIM-MM-DCSK system is obtained as

$$
\mathbf{G} = \begin{bmatrix} \mathbf{g}_0 \\ \mathbf{g}_1 \\ \mathbf{g}_2 \\ \vdots \\ \mathbf{g}_i \\ \vdots \\ \mathbf{g}_{N_T} \end{bmatrix}, \tag{5}
$$

where $\mathbf{g}_0 = \mathbf{1}_{1 \times M_T} \otimes \mathbf{c}_x$ denotes the reference signal and $\otimes$ is the Kronecker product. $\mathbf{g}_i = \begin{cases} \mathbf{U}_k, & v_s(i)=1 \\ \mathbf{W}_k, & v_s(i)=0 \end{cases}$ denotes the information-bearing signal corresponding to the ith subcarrier. The discrete signals are processed by the pulse shaping filters and the resultant signals are modulated by the specific subcarriers according to the subcarrier index vector $\mathbf{v}_s$. Consequently, the transmitted signal after pulse shaping and carrier modulation is obtained as

$$
e(t) = g_0(t)\cos(2\pi f_0 t) + \sum_{i=1}^{N_T} g_i(t)\cos(2\pi f_i t), \tag{6}
$$

where $g_0(t)$ and $g_i(t)$ denote the analog reference and information-bearing signals, respectively. Note that after passing through the pulse shaping filter, the discrete signals $\mathbf{g}_0$ and $\mathbf{g}_i, i = 1, 2, \cdots, N_T$, in (5) are converted to the analog signals $g_0(t)$ and $g_i(t)$. Moreover, a square-root-raised-cosine filter [45] is used. The length of the transmitted signal within each subcarrier is the same as the spreading factor, namely $\beta = M_T\theta$. Furthermore, f_0 and f_i are the frequency of the reference subcarrier and the ith information-bearing subcarrier, respectively. For clarity, the main parameters of the JTFIM-MM-DCSK system and their meanings are tabulated in Table I.

B. The Receiver

In this paper, we consider an L-path Rayleigh fading channel with the channel coefficient λ_l and time delay τ_l [11],

This article has been accepted for publication in a future issue of this journal, but has not been fully edited. Content may change prior to final publication. Citation information: DOI 10.1109/TWC.2021.3062836, IEEE Transactions on Wireless Communications

The final version of record is available at   http://dx.doi.org/10.1109/TWC.2021.3062836

5

TABLE I
MAIN PARAMETERS AND THEIR MEANINGS

| Parameters	Meanings
N_T	The number of all information-bearing subcarriers
N_S	The number of selected subcarriers
M_T	The number of all time slots per subcarrier
M_S	The number of selected time slots per subcarrier
κ	The number of transmitted bits per JTFIM-MM-DCSK symbol
κ_1	The number of carrier index bits
κ_2	The number of time slot index bits within a selected subcarrier
κ_3	The number of modulated bits conveyed by the unselected subcarriers
κ_4	The number of modulated bits transmitted by a selected subcarrier
$d_i \mathbf{c}_x$	Signal mode 1 transmitted by the selected time slots within the selected subcarriers
$a_i \mathbf{c}_x + b_i \mathbf{c}_y$	Signal mode 2 transmitted by the unselected time slots within the selected subcarriers
$q_i \mathbf{c}_y$	Signal mode 3 transmitted by the unselected subcarriers
β	The spreading factor of the JTFIM-MM-DCSK system
θ	The length of the initial chaotic signal produced by the chaotic generator
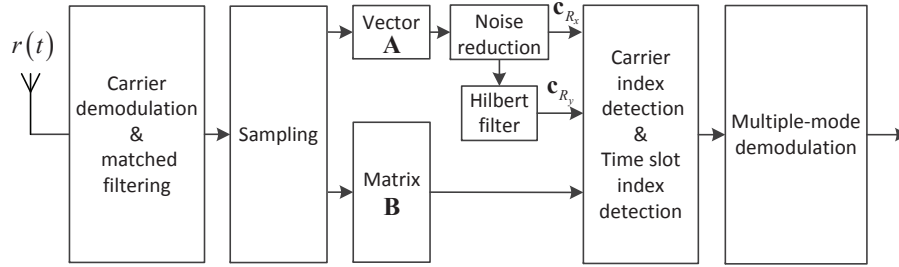
Fig. 4.   Block diagram of JTFIM-MM-DCSK receiver.

[12]. When the transmitted signal passes through the fading channel and the resultant signal is polluted by additive white Gaussian noise (AWGN), the received signal is formulated by

$$r(t) = \sum_{l=1}^{L} \lambda_l e(t - \tau_l) + n(t), \qquad (7)$$

where $n(t)$ denotes an AWGN with zero mean and $N_0/2$ variance. In general, when $L = 1$, $\lambda_1 = 1$ and $\tau_1 = 0$, the fading channel degrades to an AWGN channel. Here, it is assumed that the largest multipth delay is much short than the spreading factor, so that the inter-symbol interference (ISI) can be ignored. Moreover, the carrier synchronization within the JTFIM-MM-DCSK receiver is assumed to be perfect, and therefore the inter-carrier interference (ICI) is negligible.

Fig. 4 depicts the block diagram of the JTFIM-MM-DCSK receiver. The received signal is processed by the carrier demodulation and matched filtering so as to extract the reference and information-bearing signals within different subcarriers. Subsequently, the resultant signals are loaded into sampling block to obtain the corresponding discrete signals. After the above process is completed, the reference signal is stored in vector $\mathbf{A}$, while the information-bearing signals are placed in matrix $\mathbf{B}$. Thus, the signals within $\mathbf{A}$ and $\mathbf{B}$ can be expressed as

$$\mathbf{A} = [\mathbf{r}_{x,1}, \mathbf{r}_{x,2}, \cdots, \mathbf{r}_{x,M_T}], \qquad (8)$$

$$\mathbf{B} = \begin{bmatrix} \mathbf{r}_{1,1} & \cdots & \mathbf{r}_{1,M_T} \\ \vdots & \ddots & \vdots \\ \mathbf{r}_{N_T,1} & \cdots & \mathbf{r}_{N_T,M_T} \end{bmatrix}, \qquad (9)$$

where $\mathbf{r}_{x,i}$ is the received referecne signal within the ith time slot. Moreover, $\mathbf{r}_{i,j}$ denotes the information-bearing signal within the jth time slot carried by the ith subcarrier. To suppress the noise within the reference signal, a classical noise reduction algorithm [51] is applied. After processed by the noise reduction algorithm, the reference signal is obtained as

$$\mathbf{c}_{R_x} = \frac{1}{M_T} \sum_{i=1}^{M_T} \mathbf{r}_{x,i} = \sum_{l=1}^{L} \lambda_l \mathbf{c}_{x,\tau_l} + \mathbf{n}_{R_x}, \qquad (10)$$

where $\mathbf{n}_{R_x}$ denotes an AWGN with zero mean and $N_0/(2M_T)$ variance. The orthogonal signal of $\mathbf{c}_{R_x}$ is $\mathbf{c}_{R_y}$, given by $\mathbf{c}_{R_y} = \sum_{l=1}^{L} \lambda_l \mathbf{c}_{y,\tau_l} + \mathbf{n}_{R_y}$, where $\mathbf{n}_{R_y}$ denotes a noise having the same mean and variance as $\mathbf{n}_{R_x}$.

In order to recover the information bits, the JTFIM-MM-DCSK receiver needs to determine the positions of the selected subcarriers and time slots and then retrieves the carrier index bits, time slot index bits and modulated bits within the selected and unselected subcarriers. For this purpose, an effective index detection algorithm is proposed, as shown in **Algorithm 1**. Firstly, the algorithm is initialized by $\mathbf{C}_{R_x}$, $\mathbf{C}_{R_y}$, $\mathbf{B}$, N_S and M_S, where $\mathbf{C}_{R_x}$ is obtained by extending the signal

---

Algorithm 1 Index Detection Algorithm

Input: $\mathbf{C}_{R_x}$, $\mathbf{C}_{R_y}$, $\mathbf{B}$, N_S and M_S;

    Carrier Index Detection

1: $\mathbf{D} = \mathbf{C}_{R_x} \odot \mathbf{B}$;
2: **for** $i = 1 : N_S$
3:      $[r_s, c_s] = \text{find}\{|\mathbf{D}| == \max[\max(|\mathbf{D}|)]\}$;
4:      $\mathbf{D}(r_s, :) = 0$;
5:      $\mathbf{J}_s(i) = r_s$;
6: **end for**
7: The carrier index bits are recovered by the N_S indices $\mathbf{J}_s$.

    Time Slot Index Detection

8: $\mathbf{L} = \mathbf{C}_{R_y} \odot \mathbf{B}$;
9: **for** $i = 1 : N_S$
10:      $\mathbf{K} = \mathbf{L}(\mathbf{J}_s(i), :)$;
11:      **for** $j = 1 : M_S$
12:          $[r_p, c_p] = \min(|\mathbf{K}|)$;
13:          $\mathbf{K}(:, c_p) = +\infty$;
14:          $\mathbf{J}_p(i, j) = c_p$;
15:      **end for**
16: **end for**
17: All time slot index bits are obtained with the aid of the $N_S M_S$ indices $\mathbf{J}_p$.

Output: The specific indices of the selected subcarriers and time slots, and the carrier and time slot index bits.

$\mathbf{c}_{R_x}$, namely $\mathbf{C}_{R_x} = \mathbf{1}_{N_T \times 1} \otimes (\mathbf{1}_{1 \times M_T} \otimes \mathbf{c}_{R_x})$. Similarly, $\mathbf{C}_{R_y} = \mathbf{1}_{N_T \times 1} \otimes (\mathbf{1}_{1 \times M_T} \otimes \mathbf{c}_{R_y})$. Then, in order to determine the indices of the selected subcarriers, the element of $\mathbf{C}_{R_x}$ is multiplied by $\mathbf{B}$, i.e.,

$$\mathbf{D} = \mathbf{C}_{R_x} \odot \mathbf{B} = \begin{bmatrix} \mathbf{c}_{R_x}(\mathbf{r}_{1,1})^T & \cdots & \mathbf{c}_{R_x}(\mathbf{r}_{1,M_T})^T \\ \vdots & \ddots & \vdots \\ \mathbf{c}_{R_x}(\mathbf{r}_{N_T,1})^T & \cdots & \mathbf{c}_{R_x}(\mathbf{r}_{N_T,M_T})^T \end{bmatrix}, \quad (11)$$

in which $\odot$ denotes the multiplication of the block matrix and $(\cdot)^T$ is the transpose operation. Secondly, N_S maximum values of $|\mathbf{D}|$ are found. If the first maximum values of $|\mathbf{D}|$ is located in the ith row and j^{th} column, and the row index i is recorded as the index of the selected subcarrier, then let the elements of the ith row of $\mathbf{D}$ be zero, i.e., $\mathbf{D}(i, :) = 0$. Subsequently, other carrier indices are obtained based on the modified matrix $\mathbf{D}$. In addition, the corresponding subcarrier indices of these maximum values of $|\mathbf{D}|$ are stored in the index vector of the selected subcarriers $\mathbf{J}_s$. The carrier index bits are recovered by the N_S indices stored in $\mathbf{J}_s$ with the aid of the reverse combinational method. Specifically, the principle of the reverse combinational method [50] is clarified as follows: After obtaining $\mathbf{J}_s$, i.e., $\mathbf{J}_s = [J_{s,1}, \cdots, J_{s,2}, J_{s,N_s}]$, it is easy to get the decimal number $\tilde{Z}$ using (2). Finally, the carrier index bits can be retrieved by converting $\tilde{Z}$ from the decimal number to the binary bits.

After determining the positions of the selected subcarriers, the time slot index detection is performed to obtain the specific indices of the selected time slots. In the time slot index detection, the signal $\mathbf{C}_{R_y}$ is first multiplied by $\mathbf{B}$, i.e., $\mathbf{L} = \mathbf{C}_{R_y} \odot \mathbf{B}$. Considering the ith selected subcarrier, the
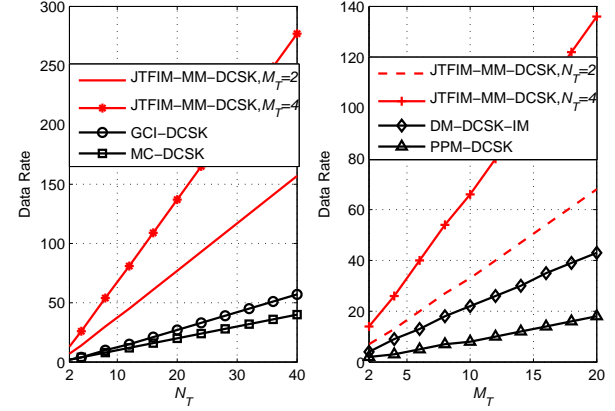

Fig. 5. Data rate comparison of the JTFIM-MM-DCSK and other chaotic communication systems with various N_T and M_T. $N_S = \frac{1}{2}N_T$ and $M_S = \frac{1}{2}M_T$.

corresponding decision variable is given as $\mathbf{K} = \mathbf{L}(\mathbf{J}_s(i), :)$. After ascertaining the M_S minimum values of $|\mathbf{K}|$, the specific indices of these minimum values, stored in $\mathbf{J}_p$, are obtained. At this point, the time slot index bits within the ith selected subcarrier can be regained by using the reverse combinational method. After N_S time loops, all time slot index bits can be recovered successfully. Once the indices of the selected subcarriers and time slots are obtained, the receiver knows the positions of subcarriers and time slots, which are used to convey signals in different modes. At this moment, the multiple-mode demodulator is applied to recover the modulated bits corresponding to signals in various modes.

III. SYSTEM ANALYSIS

A. Data Rate Comparison

In order to confirm the advantage of high data rate for the JTFIM-MM-DCSK system, the data rate of the proposed system is compared with that of other chaotic communication systems. Generally, the total number of transmitted bits per symbol is defined as the data rate. Since all resources of subcarriers and time slots are fully exploited, the JTFIM-MM-DCSK system makes great progress in terms of pursuing high-data-rate transmission. According to the analysis of the above subsections, the data rate of the JTFIM-MM-DCSK system is given as $\aleph_1 = \lfloor \log_2 \binom{N_T}{N_S} \rfloor + N_S \lfloor \log_2 \binom{M_T}{M_S} \rfloor + (N_T - N_S)M_T + N_S[M_S + 2(M_T - M_S)]$. Specifically, the number of carrier index bits is $\lfloor \log_2 \binom{N_T}{N_S} \rfloor$, while the total number of time slot index bits is $N_S \lfloor \log_2 \binom{M_T}{M_S} \rfloor$. The numbers of transmitted bits for signals of mode 1, 2 and 3 are $N_S M_S$, $N_S(2M_T - M_S)$ and $(N_T - N_S)M_T$, respectively. In addition, the data rates of the GCI-DCSK, MC-DCSK, DM-DCSK-IM and PPM-DCSK systems are obtained as $\aleph_2 = \lfloor \log_2 \binom{N_T}{N_S} \rfloor + N_S$, $\aleph_3 = N_T$, $\aleph_4 = \lfloor \log_2 M_T \rfloor + [1 + 2(M_T - 1)]$ and $\aleph_5 = \lfloor \log_2 M_T \rfloor + 1$, respectively.

Fig. 5 compares the data rate of the JTFIM-MM-DCSK system with that of its rivals, where $N_S = \frac{1}{2}N_T$ and $M_S = \frac{1}{2}M_T$. As observed, the JTFIM-MM-DCSK system achieves the highest data rate in contrast to other chaotic
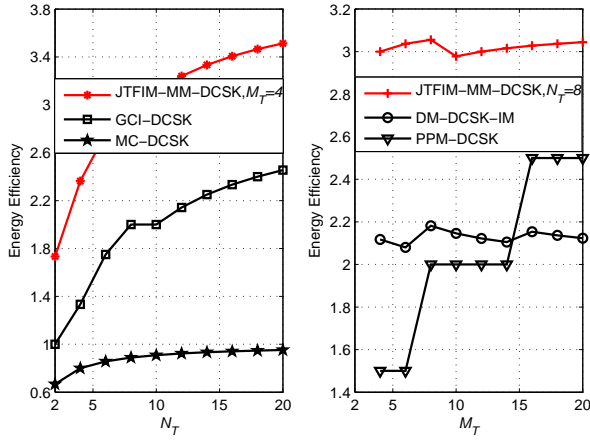
Fig. 6. Energy efficiency comparison of the JTFIM-MM-DCSK and other chaotic communication systems with different N_T and M_T. $N_S = \frac{1}{2}N_T$ and $M_S = \frac{1}{2}M_T$.

Fig. 7. Spectral efficiency comparison of the JTFIM-MM-DCSK and other chaotic communication systems with different N_T and M_T. $N_S = \frac{1}{2}N_T$, $M_S = \frac{1}{2}M_T$ and $\theta B = 50$.

communication systems under the conditions of different N_T and M_T. For example, when $N_T = 40$ and $M_T = 2$, the data rate of the JTFIM-MM-DCSK system is almost three times of the GCI-DCSK system. A more than five-fold improvement of the data rate is achieved in the JTFIM-MM-DCSK system compared to the GCI-DCSK system when $N_T = 40$ and $M_T = 4$.

B. Energy Efficiency and Spectral Efficiency

In this paper, the amount of data transmission per energy (DTE) is used as an effective indicator to evaluate the energy efficiency of chaotic communication systems. Clearly, the value of DTE is the reciprocal of bit energy. Therefore, the definition of DTE is given by

$$DTE = \frac{D_s}{E_s} = \frac{1}{E_b}, \qquad (12)$$

where D_s is the overall amount of data transmission within a symbol period and E_s denotes the symbol energy. According to the signal format of the proposed JTFIM-MM-DCSK system, the symbol energy of the system is $E_s = \{M_T + \frac{1}{4}(N_T - N_s)M_T + N_s[M_T - \frac{3}{4}M_S]\}\sum_{k=1}^{\theta} E[x_k^2]$. When the energy of the chaotic signal is normalized, i.e., $\sum_{k=1}^{\theta} E[x_k^2] = 1$, the energy efficiency of the JTFIM-MM-DCSK system is obtained as

$$DTE_1 = \frac{\kappa_1 + N_S\kappa_2 + \kappa_3 + N_S\kappa_4}{M_T + \frac{1}{4}(N_T - N_s)M_T + N_s\left[M_T - \frac{3}{4}M_S\right]}. \qquad (13)$$

Similarly, according to [41], [44], [45] and [47], the energy efficiency of the GCI-DCSK, MC-DCSK, DM-DCSK-IM and PPM-DCSK systems are given by $DTE_2 = \frac{\lfloor \log_2\binom{N_T}{N_S} \rfloor + N_S}{1 + N_S}$, $DTE_3 = \frac{N_T}{1 + N_T}$, $DTE_4 = \frac{\lfloor \log_2 M_T \rfloor + [1 + 2(M_T - 1)]}{\frac{1}{4} + M_T}$ and $DTE_5 = \frac{\lfloor \log_2 M_T \rfloor + 1}{2}$, respectively. Fig. 6 shows the energy efficiency of the JTFIM-MM-DCSK and other chaotic communication systems. It is clear that the proposed JTFIM-MM-DCSK system achieves the highest energy efficiency in contrast to its competitors.

Spectral efficiency is also another important index to assess the system performance. In this paper, the ratio of bit rate to total bandwidth is used to evaluate the spectral efficiency. Accordingly, the spectral efficiency of the JTFIM-MM-DCSK system is given by $SE_1 = \frac{\kappa_1 + N_S\kappa_2 + \kappa_3 + N_S\kappa_4}{(1 + N_T)M_T\theta B}$, where B is the bandwidth of the subcarrier. Moreover, the spectral efficiency of the GCI-DCSK, MC-DCSK, DM-DCSK-IM and PPM-DCSK systems are obtained as $SE_2 = \frac{\lfloor \log_2\binom{N_T}{N_S} \rfloor + N_S}{(1 + N_T)\theta B}$, $SE_3 = \frac{N_T}{(1 + N_T)\theta B}$, $SE_4 = \frac{\lfloor \log_2 M_T \rfloor + [1 + 2(M_T - 1)]}{(1 + M_T)\theta B}$ and $SE_5 = \frac{\lfloor \log_2 M_T \rfloor + 1}{(1 + M_T)\theta B}$, respectively. The spectral efficiency of the proposed JTFIM-MM-DCSK system and other chaotic communication systems are plotted in Fig. 7. Clearly, the spectral efficiency of the JTFIM-MM-DCSK system is better than that of the GCI-DCSK, MC-DCSK and PPM-DCSK systems, but worse than that of the DM-DCSK-IM system.

C. System Complexity

In this subsection, the system complexity of the JTFIM-MM-DCSK system is evaluated and compared to other chaotic communication systems, including the GCI-DCSK, MC-DCSK, DM-DCSK-IM and PPM-DCSK systems. Generally, the total number of multiplication operations in the modulation and demodulation processes is used to evaluate the system complexity. At the JTFIM-MM-DCSK transmitter, $(N_T - N_S)M_T\theta + N_S[M_S + 2(M_T - M_S)]\theta$ multiplications are needed to modulate signals of mode 1, 2 and 3. In order to retrieve the carrier indices and time slot indices, the JTFIM-MM-DCSK receiver needs to perform $2N_TM_T\theta$ multiplication operations. After that, $(N_T - N_S)M_T\theta + N_S[M_S + 2(M_T - M_S)]\theta$ multiplications are used to demodulate the information bits within different signal modes. Therefore, the system complexity of the JTFIM-MM-DCSK system can be calculated as

$$\mathcal{O}_1 = 2\{(N_T - N_S)M_T + N_S[M_S + 2(M_T - M_S)] + N_TM_T\}\theta. \qquad (14)$$
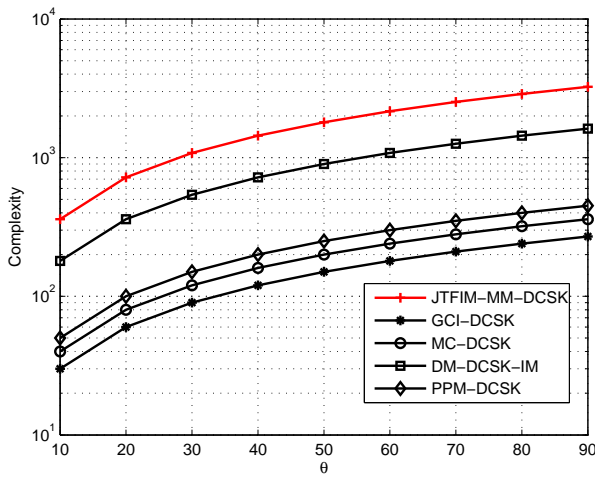
Fig. 8. System complexity comparison of the JTFIM-MM-DCSK and other chaotic communication systems with different θ. In addition, $N_T = 2$, $N_S = 1$, $M_T = 4$ and $M_S = 2$.

Similarly, the complexity of the GCI-DCSK, MC-DCSK, DM-DCSK-IM and PPM-DCSK systems can be obtained as $\mathcal{O}_2 = (N_S + N_T)\theta$, $\mathcal{O}_3 = 2N_T\theta$, $\mathcal{O}_4 = \{2[1 + 2(M_T - 1)] + M_T\}\theta$ and $\mathcal{O}_5 = (1 + M_T)\theta$, respectively. As shown in Fig. 8, the system complexity of the aforementioned systems goes up with increasing θ. Clearly, the proposed JTFIM-MM-DCSK system has higher system complexity compared to other chaotic communication systems.

IV. PERFORMANCE ANALYSIS

In order to retrieve all information bits successfully, the JTFIM-MM-DCSK receiver needs to perform the following three tasks: (1) Firstly, after determining the positions of the selected subcarriers, the carrier index bits are recovered. Then, the modulated bits within the unselected subcarriers are demodulated by the multiple-mode DCSK demodulator. (2) Secondly, the positions of the selected time slots within the selected subcarriers are sought out to regain the time slot index bits. (3) Thirdly, the modulated bits of the selected and unselected time slots are retrieved by the multiple-mode DCSK demodulator.

1) Error Probability of the Carrier Index Detection: According to the principle of the JTFIM-MM-DCSK receiver, the decision variable corresponding to the correct carrier index detection is obtained as

$$D_c^i \approx \left[\sum_{l=1}^{L} \lambda_l \mathbf{c}_{x,\tau_l} + \mathbf{n}_{R_x}\right]\left[\sum_{l=1}^{L} \lambda_l \left(a_i \mathbf{c}_{x,\tau_l} + b_i \mathbf{c}_{y,\tau_l}\right) + \mathbf{n}_I\right]^T$$

$$= \sum_{l=1}^{L} \lambda_l^2 \mathbf{c}_{x,\tau_l}(a_i \mathbf{c}_{x,\tau_l} + b_i \mathbf{c}_{y,\tau_l})^T + \sum_{l=1}^{L} \lambda_l \mathbf{c}_{x,\tau_l}(\mathbf{n}_I)^T$$

$$+ \sum_{l=1}^{L} \lambda_l \mathbf{n}_{R_x}(a_i \mathbf{c}_{x,\tau_l} + b_i \mathbf{c}_{y,\tau_l})^T + \mathbf{n}_{R_x}(\mathbf{n}_I)^T, \quad (15)$$

where $\mathbf{n}_I$ denotes the noise with zero mean and variance $N_0/2$ within the information-bearing signal. The mean and variance

of decision variable D_c^i can be computed by

$$\mathrm{E}\left[D_c^i\right] \approx \sum_{l=1}^{L} \lambda_l^2 a_i \mathrm{E}\left[\mathbf{c}_{x,\tau_l}(\mathbf{c}_{x,\tau_l})^T\right] = a_i E_c = \mu_1, \quad (16)$$

$$\mathrm{Var}\left[D_c^i\right] \approx \sum_{l=1}^{L} \lambda_l^2 \mathrm{Var}\left[\mathbf{c}_{x,\tau_l}(\mathbf{n}_I)^T\right] + \mathrm{Var}\left[\mathbf{n}_{R_x}(\mathbf{n}_I)^T\right]$$

$$+ \sum_{l=1}^{L} \lambda_l^2 \mathrm{Var}\left[\mathbf{n}_{R_x}(a_i \mathbf{c}_{x,\tau_l} + b_i \mathbf{c}_{y,\tau_l})^T\right]$$

$$= \frac{E_c N_0}{2}\left(\frac{a_i^2 + b_i^2}{M_T} + 1\right) + \theta \frac{N_0^2}{4M_T} = \sigma_1^2, \quad (17)$$

where $E_c = \sum_{l=1}^{L} \lambda_l^2 \mathrm{E}[\mathbf{c}_{x,\tau_l}(\mathbf{c}_{x,\tau_l})^T]$. In addition, $\mathrm{E}[\cdot]$ and $\mathrm{Var}[\cdot]$ are the mean and variance operations, respectively. The symbol energy of the JTFIM-MM-DCSK system is given by $E_s = \rho E_c$, where

$$\rho = M_T + q_i^2(N_T - N_s)M_T$$
$$+ N_s\left[d_i^2 M_S + (a_i^2 + b_i^2)(M_T - M_S)\right], \quad (18)$$

When the carrier index detection is incorrect, the corresponding decision variable is expressed as

$$D_e^i \approx \left(\sum_{l=1}^{L} \lambda_l \mathbf{c}_{x,\tau_l} + \mathbf{n}_{R_x}\right)\left(\sum_{l=1}^{L} \lambda_l q_i \mathbf{c}_{y,\tau_l} + \mathbf{n}_I\right)^T \quad (19)$$

with mean $\mathrm{E}\left[D_e^i\right] = 0$ and variance $\mathrm{Var}\left[D_e^i\right] = \frac{E_c N_0}{2}\left(\frac{q_i^2}{M_T} + 1\right) + \theta \frac{N_0^2}{4M_T} = \sigma_2^2$, respectively.

When the minimum absolute value of the decision variables $D_c^i, i = 1, 2, \cdots, N_S$, corresponding to the correct carrier index detection, is larger than that of the maximum absolute value of the incorrect ones, $D_e^i, i = 1, 2, \cdots, N_T - N_S$, the carrier index detection will be correct. Accordingly, the error probability of the carrier index detection is given by

$$P_d^C = \int_0^\infty \left\{1 - \left[F_{|D_e^i|}(y)\right]^{N_T - N_S}\right\}$$
$$\times N_S\left[1 - F_{|D_c^i|}(y)\right]^{N_S - 1} f_{|D_c^i|}(y)\,\mathrm{d}y, \quad (20)$$

where $F_{|D_e^i|}(y)$ and $F_{|D_c^i|}(y)$ denote the cumulative distribution function (CDF) of $\left|D_e^i\right|$ and $\left|D_c^i\right|$, respectively, while $f_{|D_c^i|}(y)$ represents the probability density function (PDF) of $\left|D_c^i\right|$. Since the decision variables D_c^i and D_e^i can be regarded as Gaussian variables approximately, the absolute values of D_c^i and D_e^i follow the folded Gaussian distribution. Therefore,

$$f_{|D_c^i|}(y) = \frac{1}{\sqrt{2\pi\sigma_1^2}}\left(e^{-\frac{(y-\mu_1)^2}{2\sigma_1^2}} + e^{-\frac{(y+\mu_1)^2}{2\sigma_1^2}}\right)$$
$$= \hbar\left(y; \mu_1, \sigma_1^2\right) \quad (21)$$

$$F_{|D_c^i|}(y) = \frac{1}{2}\left[\mathrm{erf}\left(\frac{x+\mu_1}{\sqrt{2\sigma_1^2}}\right) + \mathrm{erf}\left(\frac{x-\mu_1}{\sqrt{2\sigma_1^2}}\right)\right]$$
$$= \lambda\left(y; \mu_1, \sigma_1^2\right) \quad (22)$$

$$F_{|D_e^i|}(y) = \lambda\left(y; 0, \sigma_2^2\right), \quad (23)$$

where $\mathrm{erf}(x) = \frac{2}{\sqrt{\pi}}\int_0^x e^{-t^2}\,\mathrm{d}t, x \geq 0$ is the error function. According to [52], the BER of the carrier index bits can be obtained as $P_{map}^C = \frac{2^{(\kappa_1-1)}}{2^{\kappa_1}-1} P_d^C$.

TABLE II
DECISION VARIABLES AND THEIR MEANS AND VARIANCES.

Decision variables	Z_q^i	Z_d^i	Z_a^i
Means	$\mu_3 = q_i E_c$	$\mu_4 = d_i E_c$	μ_1
Variances	σ_2^2	σ_3^2	σ_1^2

2) Error Probability of the Time Slot Index Detection:
In the case of correct time slot index detection, the decision variable can be written as

$$K_c^i \approx \left(\sum_{l=1}^L \lambda_l \mathbf{c}_{y,\tau_l} + \mathbf{n}_{R_y} \right) \left(\sum_{l=1}^L \lambda_l d_i \mathbf{c}_{x,\tau_l} + \mathbf{n}_I \right)^T \quad (24)$$

with mean $\mathrm{E}\left[K_c^i\right] = 0$ and variance $\mathrm{Var}\left[K_c^i\right] = \frac{E_c N_0}{2} \left(\frac{d_i^2}{M_T} + 1 \right) + \theta \frac{N_0^2}{4 M_T} = \sigma_3^2$. When the time slot indices are detected incorrectly, the corresponding decision variable is represented as

$$K_e^i \approx \left[\sum_{l=1}^L \lambda_l \mathbf{c}_{y,\tau_l} + \mathbf{n}_{R_y} \right] \left[\sum_{l=1}^L \lambda_l \left(a_i \mathbf{c}_{x,\tau_l} + b_i \mathbf{c}_{y,\tau_l} \right) + \mathbf{n}_I \right]^T \quad (25)$$

In this case, the mean and variance of K_e^i can be calculated as $\mathrm{E}\left[K_e^i\right] = b_i E_c = \mu_2$ and $\mathrm{Var}\left[K_e^i\right] = \frac{E_c N_0}{2} \left(\frac{a_i^2 + b_i^2}{M_T} + 1 \right) + \theta \frac{N_0^2}{4 M_T} = \sigma_1^2$, respectively.

It can be clearly observed that, when the maximum absolute value of the decision variables $K_c^i, i = 1, 2, \cdots, M_S$, corresponding to the correct carrier index detection, is less than that of the minimum absolute value of the incorrect cases $K_e^i, i = 1, 2, \cdots, M_T - M_S$, the time slot index detection is correct. Consequently, the time slot index symbol is detected incorrectly with probability

$$P_d^T = \int_0^\infty \left\{ 1 - \left[F_{|K_c^i|}(y) \right]^{M_S} \right\} (M_T - M_S)$$
$$\times \left[1 - F_{|K_e^i|}(y) \right]^{M_T - M_S - 1} f_{|K_e^i|}(y)\,\mathrm{d}y, \quad (26)$$

where $F_{|K_c^i|}(y) = \lambda\left(y; 0, \sigma_3^2\right)$, $F_{|K_e^i|}(y) = \lambda\left(y; \mu_2, \sigma_1^2\right)$ and $f_{|K_e^i|}(y) = \hbar\left(y; \mu_2, \sigma_1^2\right)$. As a result, the bit error probability of the time slot index bits is obtained as $P_{map}^T = \frac{2^{(\kappa_2 - 1)}}{2^{\kappa_2} - 1} P_d^T$.

3) Error Probability of the Modulated Bits: When the carrier index detection is correct, one may first consider the modulated bits within the unselected subcarriers. In this case, the decision variable of the unselected subcarrier is given by

$$Z_q^i \approx \left(\sum_{l=1}^L \lambda_l \mathbf{c}_{y,\tau_l} + \mathbf{n}_{R_y} \right) \left(\sum_{l=1}^L \lambda_l q_i \mathbf{c}_{y,\tau_l} + \mathbf{n}_I \right)^T. \quad (27)$$

Regarding the selected subcarriers, the decision variable of the selected time slot is represented by

$$Z_d^i \approx \left(\sum_{l=1}^L \lambda_l \mathbf{c}_{x,\tau_l} + \mathbf{n}_{R_x} \right) \left(\sum_{l=1}^L \lambda_l d_i \mathbf{c}_{x,\tau_l} + \mathbf{n}_I \right)^T. \quad (28)$$

Moreover, the decision variable of the in-phase branch corresponding to the unselected time slot is obtained as

$$Z_a^i \approx \left[\sum_{l=1}^L \lambda_l \mathbf{c}_{x,\tau_l} + \mathbf{n}_{R_x} \right] \left[\sum_{l=1}^L \lambda_l \left(a_i \mathbf{c}_{x,\tau_l} + b_i \mathbf{c}_{y,\tau_l} \right) + \mathbf{n}_I \right]^T \quad (29)$$

The means and variances of Z_q^i, Z_d^i and Z_a^i are tabulated in Table II. Furthermore, let P_Q, P_D and P_A represent the bit error probabilities of the modulated bits carried by the unselected subcarriers, the modulated bits within the selected and unselected time slots transmitted by the selected subcarriers, respectively. From another point of view, P_D, P_A and P_Q also denote the BERs of signal modes 1, 2 and 3, respectively. According to [12], [14] and [53],

$$P_Q = \frac{1}{2}\mathrm{erfc}\left[\left(\frac{2\sigma_2^2}{(\mu_3)^2} \right)^{-\frac{1}{2}} \right] = \ell\left(\mu_3, \sigma_2^2\right)$$
$$= \frac{1}{2}\mathrm{erfc}\left[\left(\frac{\rho}{\gamma_s} \left(\frac{1}{M_T} + \frac{1}{q_i^2} \right) + \frac{\theta \rho^2}{2 q_i^2 M_T \gamma_s^2} \right)^{-\frac{1}{2}} \right], \quad (30)$$

where $\mathrm{erfc}(x) = \frac{2}{\sqrt{\pi}} \int_x^{+\infty} e^{-t^2}\,\mathrm{d}t$ is the complementary error function and $\gamma_s = \frac{E_s}{N_0}$ denotes the symbol signal-to-noise ratio. Similarly, $P_D = \ell\left(\mu_4, \sigma_3^2\right)$ and $P_A = \ell\left(\mu_1, \sigma_1^2\right)$.

4) BER of the JTFIM-MM-DCSK System: The overall BER of the JTFIM-MM-DCSK system is related to the BERs of the modulated bits (P_Q, P_D and P_A), the probabilities of incorrect carrier and time slot index detection (P_d^C and P_d^T) and the BERs of the carrier and time slot index bits (P_{map}^C and P_{map}^T). According to the probability theory [54], the bit error probability of the JTFIM-MM-DCSK system can be calculated by

$$P_J = \frac{\kappa_1}{\kappa_1 + N_S \kappa_2 + \kappa_3 + N_S \kappa_4} P_{map}^C$$
$$+ \frac{\kappa_3}{\kappa_1 + N_S \kappa_2 + \kappa_3 + N_S \kappa_4} P_{mod}^C$$
$$+ \frac{N_S \kappa_2}{\kappa_1 + N_S \kappa_2 + \kappa_3 + N_S \kappa_4} P_{map}^T$$
$$+ \frac{N_S \kappa_4}{\kappa_1 + N_S \kappa_2 + \kappa_3 + N_S \kappa_4} P_{mod}^T, \quad (31)$$

where P_{mod}^T denotes the BER of the modulated bits within the selected subcarriers, which can be obtained by (32) as shown at the bottom of this page. In addition, P_{mod}^C is the BER of

$$P_{mod}^T \approx \frac{M_S P_D + 2(M_T - M_S) P_A}{M_S + 2(M_T - M_S)} \left(1 - P_d^T\right) + \frac{\sum_{j=1}^{M_S} \binom{M_S}{j} \left[\frac{1}{2}(j + 2j) + (M_S - j) P_D + 2(M_T - M_S - j) P_A \right]}{\sum_{j=1}^{M_S} \binom{M_S}{j} \left[M_S + 2(M_T - M_S) \right]} P_d^T. \quad (32)$$
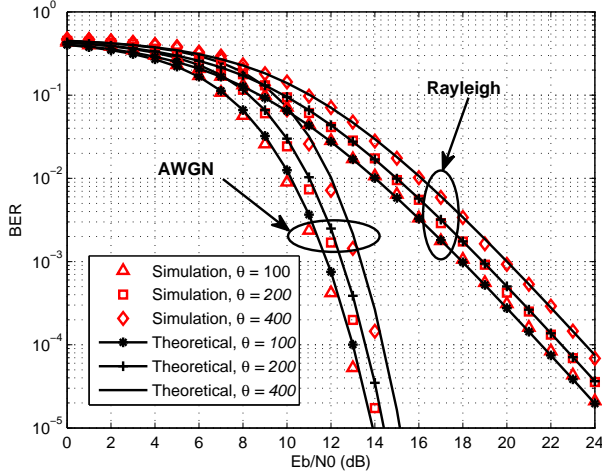
Fig. 9. The BER performance of the JTFIM-MM-DCSK system over AWGN and multipath Rayleigh fading channels. $\theta = 100, 200, 400$, $N_T = 4$, $N_S = 2$, $M_T = 4$ and $M_S = 1$.
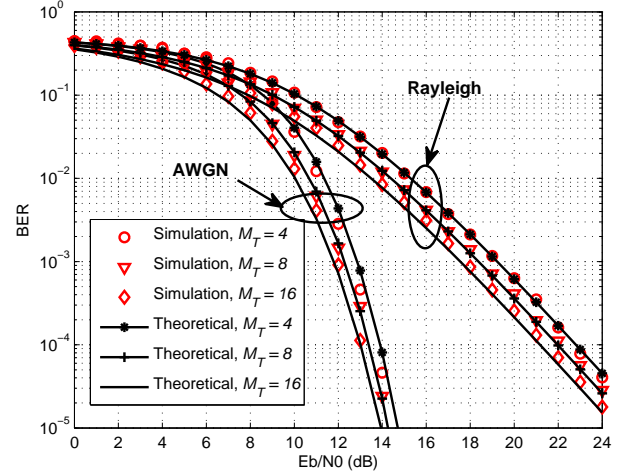

Fig. 10. The BER performance of the JTFIM-MM-DCSK system over AWGN and multipath Rayleigh fading channels. $\theta = 300$, $N_T = 4$, $N_S = 1$, $M_T = 4, 8, 16$ and $M_S = 1$.
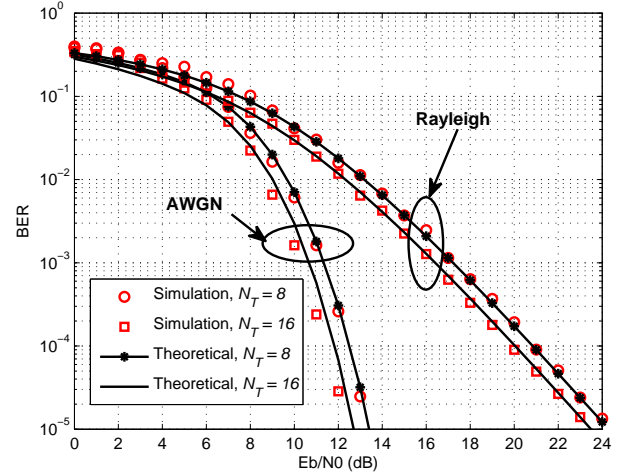
the modulated bits within the unselected subcarriers, which can be computed by

$$P_{mod}^C \approx \frac{\sum_{j=1}^{N_S} \binom{N_S}{j} \left[\frac{j}{2} M_T + (N_T - N_S - j) M_T P_Q \right]}{\sum_{j=1}^{N_S} \binom{N_S}{j} \left[(N_T - N_S) M_T \right]} P_d^C$$
$$+ P_Q \left(1 - P_d^C \right). \quad (33)$$

Therefore, the bit error probability of the JTFIM-MM-DCSK system over the multipath Rayleigh fading channel can be expressed as [11], [45]

$$\bar{P}_J = \int_0^\infty P_J(\gamma_s) \cdot \sum_{l=1}^L \frac{\Psi_l}{\bar{\gamma}_l} \exp\left(-\frac{\gamma_s}{\bar{\gamma}_l} \right) d\gamma_s, \quad (34)$$

where $\Psi_l = \prod_{j=1, j \neq l}^L \frac{\bar{\gamma}_l}{\bar{\gamma}_l - \bar{\gamma}_j}$ and $\bar{\gamma}_l$ is the average symbol SNR per channel.

V. SIMULATION RESULTS AND DISCUSSIONS

This section presents Monte Carlo simulations to demonstrate the BER performance of the proposed JTFIM-MM-DCSK system. Unless specially stated, a three-path Rayleigh fading channel with channel factors $E(\lambda_1^2) = 5/12$, $E(\lambda_2^2) = 4/12$ and $E(\lambda_3^2) = 3/12$ is applied in the simulations. The channel delays of different paths are modeled with a uniform distribution in the range of 0 to $3T_c$, where T_c is the chip duration of the chaotic signal. Furthermore, since the Logistic map $c_{k+1} = 1 - 2c_k^2, k = 1, 2, \cdots$, shows better performance [55], it is used to generate the chaotic signal for simulations.

A. Performance Evaluation

Fig. 9 shows the BER performance of the JTFIM-MM-DCSK system with different θ. It can be clearly observed that the theoretical results well match the simulated ones, verifying the theoretical expression derived in the above

Fig. 11. The BER performance of the JTFIM-MM-DCSK system over AWGN and multipath Rayleigh fading channels. $\theta = 200$, $N_T = 8, 16$, $N_S = 4$, $M_T = 16$ and $M_S = 1$.

section. As shown in Fig. 9, the BER performance of the JTFIM-MM-DCSK system is deteriorated with an increasing θ (i.e., θ increases from 100 to 400) for both AWGN and multipath Rayleigh fading channels. For instance, the JTFIM-MM-DCSK system with $\theta = 100$ has about 2dB performance gain over the case with $\theta = 400$ at a BER 10^{-4} in the multipath Rayleigh fading channel. This is mainly due to the adverse effect of the noise-to-noise cross-correlation value within the decision variable becomes more significant when θ increases.

The effect of M_T on the BER performance of the JTFIM-MM-DCSK system is shown in Fig. 10. It is easy to see that the theoretical results are in good agreement with the simulated results, thus further verifying the accuracy of the derivations. From another perspective, the JTFIM-MM-DCSK system with $M_T = 16$ has a lower BER value in contrast
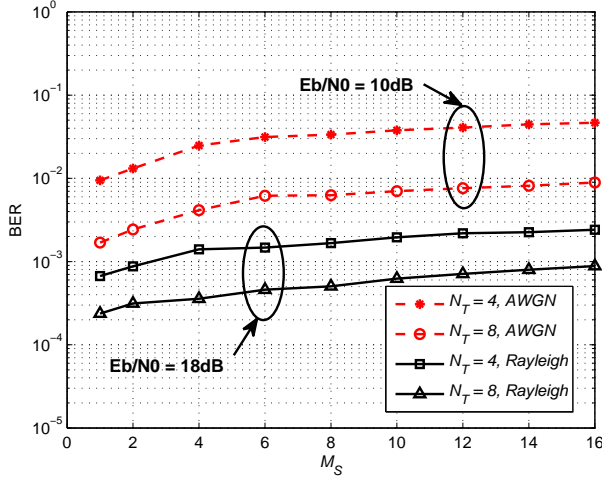
Fig. 12. The effect of M_S on the BER performance of the JTFIM-MM-DCSK system over AWGN and multipath Rayleigh fading channels. $\theta = 200$, $N_T = 4, 8$, $N_S = 1$ and $M_T = 64$.

Fig. 13. The influence of the maximum multipath delay τ_{max} on the BER performance of the JTFIM-MM-DCSK system. $E_b/N_0 = 20$dB, $\theta = 100$, $N_T = 8$, $N_S = 7$.

to that with $M_T = 4$. Specifically, the performance gain between $M_T = 16$ and $M_T = 4$ reaches to about 1dB at the BER level of 10^{-5} over the AWGN channel. In addition, this performance improvement is almost 2dB at a BER 10^{-4} in the multipath Rayleigh fading channel. The main reason is that, when more time slot index bits are transmitted with the same energy consumption, the required SNR to achieve a specific BER level would be decreased.

In addition, the effect of N_T on the BER performance of the JTFIM-MM-DCSK system is investigated in Fig. 11. The simulation results have a good fitting degree with the theoretical ones. Moreover, the JTFIM-MM-DCSK system with $N_T = 16$ performs better than that with $N_T = 8$ for both AWGN and multipath Rayleigh fading channels. It is not difficult to explain this phenomenon, i.e., a larger N_T is corresponding to more carrier index bits, which means that the saved energy used to transmit the modulated bits are increased, thereby offering the JTFIM-MM-DCSK system better BER performance. Fig. 12 shows the effect of M_S on the BER performance of the JTFIM-MM-DCSK system. It is clear that the JTFIM-MM-DCSK system has worse BER performance as M_S increases. It is because that the error probabilities of carrier and time slot index detection go up with increasing M_S, resulting in the overall BER performance degradation.

In the theoretical derivations, there was an assumption that the maximum delay time of the multipath Rayleigh fading channel is much less than the spreading factor. Here, the effect of the maximum multipath delay τ_{max} on the BER performance of the JTFIM-MM-DCSK system is shown in Fig. 13. As expected, the theoretical results match the simulation ones when τ_{max} is small. However, as τ_{max} increases continuously, the BER performance of the JTFIM-MM-DCSK system becomes worse and worse. It should be noticed that the JTFIM-MM-DCSK system with $M_T = 24$ performs better than that with $M_T = 3$ when τ_{max} is relatively small. Unfortunately, considering the increasing τ_{max}, the BER performance of the JTFIM-MM-DCSK system deteriorates quickly and the
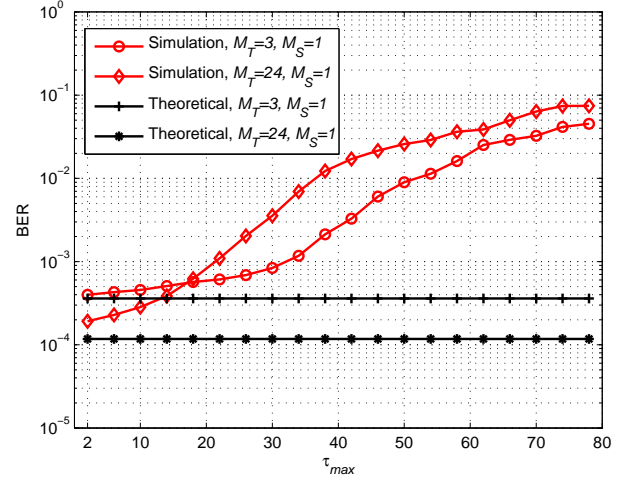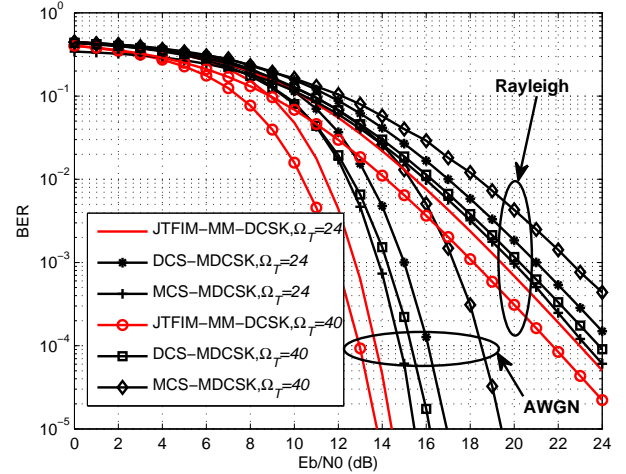

Fig. 14. The BER performances of the JTFIM-MM-DCSK, DCS-MDCSK and MCS-MDCSK systems with the same number of transmitted bits per symbol $\Omega_T = 24, 40$ and $\theta = 300$ over AWGN and multipath Rayleigh fading channels.

system with $M_T = 3$ has a lower BER compared to that with $M_T = 24$ when τ_{max} is greater than 20. In other words, the JTFIM-MM-DCSK system with a small M_T has stronger robustness against the multipath fading channel with a larger multipath delay.

B. Performance Comparison

In Fig. 14, the BER performance of the JTFIM-MM-DCSK system is compared to that of the DCS-MDCSK and MCS-MDCSK systems with the same transmitted bits per symbol $\Omega_T = 24, 40$. The main simulation parameters are: when $\Omega_T = 24$ and $\Omega_T = 40$, JTFIM-MM-DCSK system uses $N_T = 8$, $N_S = 2$, $M_T = 2$, $M_S = 1$ and $N_T = 8$, $N_S = 1$, $M_T = 4$, $M_S = 1$, respectively, while $M_p = 4$, $N_p = 5$ and $M_p = 4$, $N_p = 7$ are adopted for the DCS-MDCSK system, where M_p and N_p denote the number of the chaotic
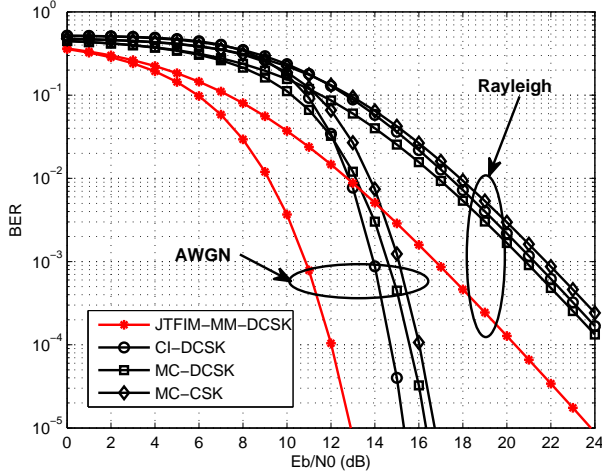
Fig. 15. The BER performances of the JTFIM-MM-DCSK, CI-DCSK, MC-DCSK and MC-CSK systems with the same number of subcarriers, $\Omega_S = 16$, and $\beta = 200$ over AWGN and multipath Rayleigh fading channels.
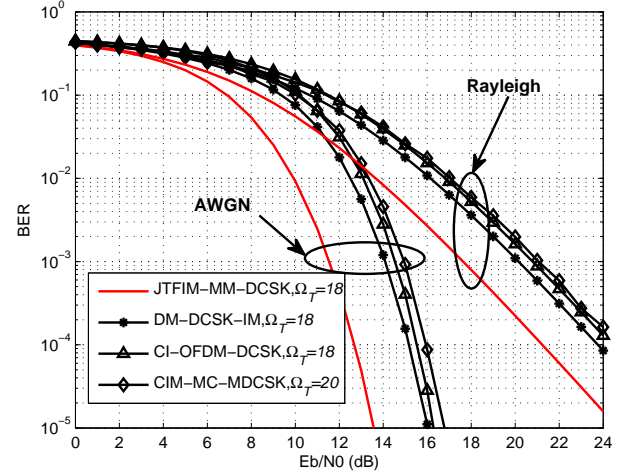

Fig. 16. The BER performances of the JTFIM-MM-DCSK, DM-DCSK-IM, CI-OFDM-DCSK and CIM-MC-MDCSK systems with $\theta = 100$ over AWGN and multipath Rayleigh fading channels.

signals and the length of the discrete cosine spreading codes. As for the MCS-MDCSK system [24], $M_o = 4$, $U_o = 12$ and $M_o = 16$, $U_o = 10$ are applied in the simulation of the MCS-MDCSK system, where U_o and M_o are the number of parallel branches and the modulation order of M-ary DCSK. As can be observed, the JTFIM-MM-DCSK system is capable of achieving 2dB performance gain better than that of the DCS-MDCSK system at the BER level of 10^{-5} over the AWGN channel. Besides, when Ω_T increases, the BER performance of MCS-MDCSK system worsens significantly, while the JTFIM-MM-DCSK system still can perform well.

In Fig. 15, the BER performance of the JTFIM-MM-DCSK system is compared with that of the CI-DCSK, MC-DCSK and MC-CSK [56] systems under the condition of the same number of subcarriers, $\Omega_S = 16$. In the simulations, $N_T = 15$, $N_S = 1$, $M_T = 2$ and $M_S = 1$ are used in the JTFIM-MM-DCSK system. As shown in Fig. 15, the JTFIM-MM-DCSK system has more than 2dB performance gain at the BER level 10^{-5} in contrast to the CI-DCSK system over AWGN channel, while this improvement increases to about 4dB in the Rayleigh fading channel. In addition, the BER performances of the JTFIM-MM-DCSK system and other state-of-the-art IM-based DCSK systems (such as DM-DCSK-IM, CI-OFDM-DCSK and CIM-MC-MDCSK systems) are compared in Fig. 16. In the JTFIM-MM-DCSK system, $N_T = 7$, $N_S = 1$, $M_T = 2$ and $M_S = 1$. It can be clearly observed that the JTFIM-MM-DCSK system achieves the best BER performance in contrast to its competitors. For example, the JTFIM-MM-DCSK system obtains more than 2dB performance gain over the DM-DCSK-IM system at 10^{-5} BER level over the AWGN channel.

The BER performances of the JTFIM-MM-DCSK, CM-DCSK and DCSK systems over the time-variant fading channel are compared in Fig. 17. Here, a three-paths Rician channel is used, whose channel coefficients are the exponentially decaying power delay profiles, $E[\lambda_l] = e^{-0.4(l-1)}$, $l = 1, 2, 3$ [57]. The channel delays are given as $\tau_1 = 0$, $\tau_2 = 2$, $\tau_3 = 4$. The ratio of specular to diffuse energy is $\wp_K = 1$. The Jakes'
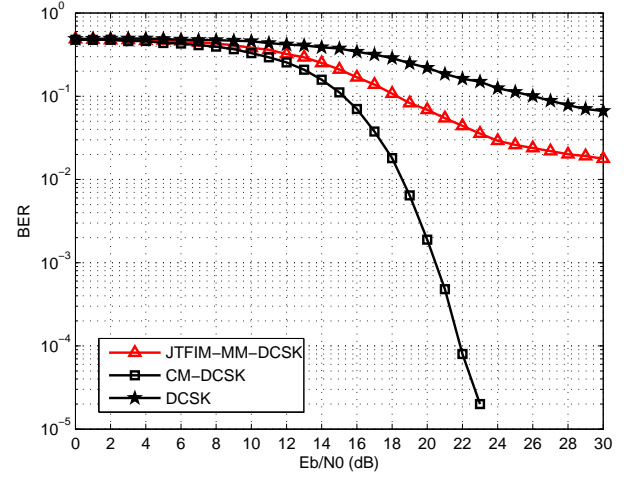

Fig. 17. The BER performances of the JTFIM-MM-DCSK, CM-DCSK and DCSK systems with $\theta = 100$ over the time-variant fading channel.

mode is used as the Doppler power spectral density of the time-variant channel. Moreover, the main parameter of the time-variant channel is $J_0(2\pi f_d T_c) = 0.7078$, where $J_0(\cdot)$ is the zeroth-order Bessel function of the first kind and f_d is the Doppler frequency [43]. The simulation parameters for the proposed JTFIM-MM-DCSK system are $N_T = 4$, $N_S = 1$, $M_T = 2$ and $M_S = 1$. In Fig. 17, it is clearly shown that the CM-DCSK system achieves much better BER performance in contrast to the JTFIM-MM-DCSK system, as the CM-DCSK system fully exploits the time diversity of wireless channels.

VI. CONCLUSIONS

Facing the current challenge of a huge demand for high-data-rate communication, a great deal of efforts have been devoted to developing novel communication schemes with high throughput. In this pursuit, a multiple-mode DCSK scheme is designed in this paper based on the joint time-frequency index

modulation. In this system, multiple-mode signals are used to transmit the information bits, while the carrier and time slot indices also offer a pair of dimensions for the transmission of additional information bits. The data rate, energy efficiency and spectral efficiency of the proposed JTFIM-MM-DCSK system are compared to other chaotic communication systems to demonstrate its advantages. The comparison results show that the JTFIM-MM-DCSK system can obtain several times higher data rate than its competitors at the expense of system complexity. Furthermore, the theoretical BERs are derived for the JTFIM-MM-DCSK system over AWGN and multipath Rayleigh fading channels. Extensive computer simulations are carried out to verify the correctness of the theoretical derivations.

Finally, when comparing the BER performance of the JTFIM-MM-DCSK system with that of other state-of-the-art chaotic communication systems, it was found that the JTFIM-MM-DCSK system achieves 2 to 5dB performance gain better than its competitors over AWGN and multipath Rayleigh fading channels. With the superiority in high data rate and strong robustness, the JTFIM-MM-DCSK system is a competitive and promising noncoherent scheme for future wireless communications. However, when a time-variant fading channel is considered, the BER performance of the JTFIM-MM-DCSK system is worse than that of the CM-DCSK system, but still better than the conventional DCSK system.

The time division multiple access (TDMA) and frequency division multiple access (FDMA) are widely used in the multiuser transmission scenarios. Similarly, the time and frequency resources within the proposed JTFIM-MM-DCSK system can be used to support multiple access transmission, and this will be our future work.

REFERENCES

[1] Y. Fang, G. Han, P. Chen, F. C. M. Lau, G. Chen, and L. Wang, "A survey on DCSK-based communication systems and their application to UWB scenarios," *IEEE Commun. Surveys Tuts.*, vol. 18, no. 3, pp. 1804-1837, 3rd Quart., 2016.

[2] G. Kaddoum, "Wireless chaos-based communication systems: A comprehensive survey," *IEEE Access*, vol. 4, pp. 2621-2648, 2016.

[3] F. C. M. Lau and C. K. Tse, *Chaos-Based Digital Communication Systems*. New York, NY, USA: Springer, 2003.

[4] U. Parlitz, L. O. Chua, L. Kocarev, K. S. Halle, and A. Shang, "Transmission of digital signals by chaotic synchronization," *Int. J. Bifurcation Chaos*, vol. 2, no. 4, pp. 973-977, 1992.

[5] H. Dedieu and M. P. Kennedy, "Chaos shift keying: Modulation and demodulation of a chaotic carrier using self-synchronization Chua's circuit," *IEEE Trans. Circuits Syst. II: Analog Digit. Signal Process.*, vol. 40, no. 10, pp. 634-642, Oct. 1993.

[6] G. Kolumbán, M. Kennedy, and L. Chua, "The role of synchronization in digital communications using chaos-Part I: Fundamentals of digital communications," *IEEE Trans. Circuits Syst. I, Reg. Papers*, vol. 44, no. 10, pp. 927-936, Oct. 1997.

[7] G. Kolumbán, M. Kennedy, and L. Chua, "The role of synchronization in digital communications using chaos-Part II: Chaotic modulation and chaotic synchronization," *IEEE Trans. Circuits Syst. I, Reg. Papers*, vol. 45, no. 11, pp. 1129-1140, Nov. 1998.

[8] G. Kolumbán and M. Kennedy, "The role of synchronization in digital communications using chaos-Part III: Performance bounds for correlation receivers," *IEEE Trans. Circuits Syst. I, Reg. Papers*, vol. 47, no. 12, pp. 1673-1683, Dec. 2000.

[9] G. Kolumbán, G. K. Vizvári, W. Schwarz, and A. Abel, "Differential chaos shift keying: A robust coding for chaos communication," in *Proc. Nonlinear Dyn. Electron. Syst.*, Seville, Spain, 1996, pp. 92-97.

[10] G. Kolumbán, M. Kennedy, G. Kis, and Z. Jako, "FM-DCSK: A novel method for chaotic communications," in *Proc. IEEE Int. Symp. Circuits Syst. (ISCAS)*, May 1998, vol. 4, pp. 477-480.

[11] Y. Xia, C. K. Tse, and F. C. M. Lau, "Performance of differential chaos-shift-keying digital communication systems over a multipath fading channel with delay spread," *IEEE Trans. Circuits Syst. II, Exp. Briefs*, vol. 51, no. 12, pp. 680-684, Dec. 2004.

[12] M. Dawa, G. Kaddoum, and Z. Sattar, "A generalized lower bound on the bit error rate of DCSK systems over multi-path Rayleigh fading channels," *IEEE Trans. Circuits Syst. II, Exp. Briefs*, vol. 65, no. 3, pp. 321-325, Mar. 2018.

[13] G. Cai and Y. Song, "Closed-form BER expressions of M-ary DCSK systems over multipath Rayleigh fading channels," *IEEE Commun. Lett.*, vol. 24, no. 6, pp. 1192-1196, June 2020.

[14] Z. Galias and G. M. Maggio, "Quadrature chaos-shift keying: Theory and performance analysis," *IEEE Trans. Circuits Syst. I, Reg. Papers*, vol. 48, no. 12, pp. 1510-1519, Dec. 2001.

[15] L. Wang, G. Cai, and G. Chen, "Design and performance analysis of a new multiresolution M-ary differential chaos shift keying communication system," *IEEE Trans. Wireless Commun.*, vol. 14, no. 9, pp. 5197-5208, Sep. 2015.

[16] G. Cai, Y. Fang, G. Han, F. C. M. Lau, and L. Wang, "A square-constellation-based M-ary DCSK sommunication system," *IEEE Access*, vol. 4, pp. 6295-6303, 2016.

[17] G. Kolumbán, Z. Jako, and M. Kennedy, "Enhanced versions of DCSK and FM-DCSK data transmission systems," in *Proc. IEEE Int. Symp. Circuits Syst. (ISCAS)*, Jul. 1999, vol. 4, pp. 475-478.

[18] H. Yang and G. Jiang, "High-efficiency differential-chaos-shift-keying scheme for chaos-based noncoherent communication," *IEEE Trans. Circuits Syst. II, Exp. Briefs*, vol. 59, no. 5, pp. 312-316, May 2012.

[19] H. Yang and G. Jiang, "Reference-modulated DCSK: A novel chaotic communication scheme," *IEEE Trans. Circuits Syst. II, Exp. Briefs*, vol. 60, no. 4, pp. 232-236, April 2013.

[20] G. Kaddoum, E. Soujeri, C. Arcila, and K. Eshteiwi, "I-DCSK: An improved non-coherent communication system architecture," *IEEE Trans. Circuits Syst. II, Exp. Briefs*, vol. 62, no. 9, pp. 901-905, Sep. 2015.

[21] G. Kaddoum, E. Soujeri and Y. Nijsure, "Design of a short reference noncoherent chaos-based communication systems," *IEEE Trans. Commun.*, vol. 64, no. 2, pp. 680-689, Feb. 2016.

[22] W. Xu, L. Wang, and G. Kolumbán, "A novel differential chaos shift keying modulation scheme," *Int. J. Bifurcation Chaos*, vol. 21, no. 3, pp. 799-814, Mar. 2011.

[23] W. Xu, L. Wang, and G. Kolumbán, "A new data rate adaption communications scheme for code-shifted differential chaos shift keying modulation," *Int. J. Bifurcation Chaos*, vol. 22, no. 8, pp. 1-8, Aug. 2012.

[24] X. Cai, W. Xu, R. Zhang, and L. Wang, "A multilevel code shifted differential chaos shift keying system with M-ary modulation," *IEEE Trans. Circuits Syst. II, Exp. Briefs*, vol. 66, no. 8, pp. 1451-1455, Aug. 2019.

[25] G. Kaddoum and F. Gagnon, "Design of a high-data-rate differential chaos-shift keying system," *IEEE Trans. Circuits Syst. II, Exp, Briefs*, vol. 59, no. 7, pp. 448-452, Jul. 2012.

[26] H. Yang, W. K. S. Tang, G. Chen, and G. Jiang, "System design and performance analysis of orthogonal multi-level differential chaos shift keying modulation scheme," *IEEE Trans. Circuits Syst. I, Reg. Papers*, vol. 63, no. 1, pp. 146-156, Jan. 2016.

[27] Z. Chen, L. Zhang and Z. Wu, "High data rate discrete-cosine-spreading aided M-ary differential chaos shift keying scheme with low PAPR," *IEEE Trans. Circuits Syst. II, Exp, Briefs*, vol. 67, no. 11, pp. 2492-2496, Nov. 2020.

[28] M. Agiwal, A. Roy and N. Saxena, "Next generation 5G wireless networks: A comprehensive survey," *IEEE Commun. Surveys Tuts.*, vol. 18, no. 3, pp. 1617-1655, thirdquarter 2016.

[29] E. Basar, M. Wen, R. Mesleh, M. Di Renzo, Y. Xiao, and H. Haas, "Index modulation techniques for next-generation wireless networks," *IEEE Access*, vol. 5, pp. 16693-16746, 2017.

[30] T. Mao, Q. Wang, Z. Wang and S. Chen, "Novel index modulation techniques: A survey," *IEEE Commun. Surveys Tuts.*, vol. 21, no. 1, pp. 315-348, Firstquarter 2019.

[31] W. Xu, T. Huang, and L. Wang, "Code-shifted differential chaos shift keying with code index modulation for high data rate transmission," *IEEE Trans. Commun.*, vol. 65, no. 10, pp. 4285-4294, Oct. 2017.

[32] X. Cai, W. Xu, D. Wang, S. Hong and L. Wang, "An M-ary orthogonal multilevel differential chaos shift keying system with code index modulation," *IEEE Trans. Commun.*, vol. 67, no. 7, pp. 4835-4847, July 2019.

This article has been accepted for publication in a future issue of this journal, but has not been fully edited. Content may change prior to final publication. Citation information: DOI 10.1109/TWC.2021.3062836, IEEE Transactions on Wireless Communications

The final version of record is available at   http://dx.doi.org/10.1109/TWC.2021.3062836

14

[33] M. Herceg, G. Kaddoum, D. Vranješ, and E. Soujeri, "Permutation index DCSK modulation technique for secure multiuser high-data-rate communication systems," *IEEE Trans. Veh. Technol.*, vol. 67, no. 4, pp. 2997-3011, Apr. 2018.

[34] M. Herceg, D. Vranješ, G. Kaddoum, and E. Soujeri, "Commutation code index DCSK modulation technique for high-data-rate communication systems," *IEEE Trans. Circuits Syst., II, Exp. Briefs*, vol. 65, no. 12, pp. 1954-1958, Dec. 2018.

[35] L. Zhang, Z. Chen, W. Rao and Z. Wu, "Efficient and secure noncoherent OFDM-based overlapped chaotic chip position shift keying system: Design and performance analysis," *IEEE Trans. Circuits Syst. I, Reg. Papers*, vol. 67, no. 1, pp. 309-321, Jan. 2020.

[36] G. Kaddoum, "Design and performance analysis of a multiuser OFDM based differential chaos shift keying communication system," *IEEE Trans. Commun.*, vol. 64, no. 1, pp. 249-260, Jan. 2016.

[37] Z. Liu, L. Zhang, Z. Wu and J. Bian, "A secure and robust frequency and time diversity aided OFDM-DCSK modulation system not requiring channel state information," *IEEE Trans. Commun.*, vol. 68, no. 3, pp. 1684-1697, March 2020.

[38] C. Bai, H. Ren and G. Kolumbán, "Double-sub-stream M-ary differential chaos shift keying wireless communication system using chaotic shape-forming filter," *IEEE Trans. Circuits Syst. I, Reg. Papers*, vol. 67, no. 10, pp. 3574-3587, Oct. 2020.

[39] Z. Liu, L. Zhang and Z. Chen, "Low PAPR OFDM-based DCSK design with carrier interferometry spreading codes," *IEEE Commun. Lett.*, vol. 22, no. 8, pp. 1588-1591, Aug. 2018.

[40] Z. Liu, L. Zhang, Z. Wu and Y. Jiang, "Energy efficient parallel concatenated index modulation and M-ary PSK aided OFDM-DCSK communications with QoS consideration," *IEEE Trans. Veh. Technol.*, vol. 69, no. 9, pp. 9469-9482, Sept. 2020.

[41] M. Miao, L. Wang, M. Katz, and W. Xu, "Hybrid modulation scheme combining PPM with differential chaos shift keying modulation," *IEEE Wireless Commun. Lett.*, vol. 8, no. 2, pp. 340-343, Apr. 2019.

[42] H. Ma, G. Cai, Y. Fang, P. Chen and G. Chen, "Design of a superposition coding PPM-DCSK system for downlink multi-user transmission," *IEEE Trans. Veh. Technol.*, vol. 69, no. 2, pp. 1666-1678, Feb. 2020.

[43] F. J. Escribano, G. Kaddoum, A. Wagemakers and P. Giard, "Design of a new differential chaos-shift-keying system for continuous mobility," *IEEE Trans. Commun.*, vol. 64, no. 5, pp. 2066-2078, May 2016.

[44] X. Cai, W. Xu, S. Hong and L. Wang, "Dual-mode differential chaos shift keying with index modulation," *IEEE Trans. Commun.*, vol. 67, no. 9, pp. 6099-6111, Sept. 2019.

[45] G. Kaddoum, F. Richardson, F. Gagnon, "Design and analysis of a multicarrier differential chaos shift keying communication system," *IEEE Trans. Commun.*, vol. 61, no. 8, pp. 3281-3291, Aug. 2013.

[46] G. Cheng, L. Wang, W. Xu, and G. Chen, "Carrier index differential chaos shift keying modulation," *IEEE Trans. Circuits Syst., II, Exp. Briefs*, vol. 64, no. 8, pp. 907-911, Aug. 2017.

[47] G. Cheng, X. Chen, W. Liu and W. Xiao, "GCI-DCSK: Generalized carrier index differential chaos shift keying modulation," *IEEE Commun. Lett.*, vol. 23, no. 11, pp. 2012-2016, Nov. 2019.

[48] G. Cheng, L. Wang, Q. Chen, and G. Chen, "Design and performance analysis of generalised carrier index M-ary differential chaos shift keying modulation," *IET Commun.*, vol. 12, no. 11, pp. 1324-1331, Jun. 2018.

[49] G. Cai, Y. Fang, J. Wen, S. Mumtaz, Y. Song and V. Frascolla, "Multicarrier M-ary DCSK system with code index modulation: An efficient solution for chaotic communications," *IEEE J. Sel. Topics Signal Process.*, vol. 13, no. 6, pp. 1375-1386, Oct. 2019.

[50] E. Başar, Ü. Aygölü, E. Panayırcı and H. V. Poor, "Orthogonal frequency division multiplexing with index modulation," *IEEE Trans Signal Process.*, vol. 61, no. 22, pp. 5536-5549, Nov.15, 2013.

[51] G. Kaddoum and E. Soujeri, "NR-DCSK: A noise reduction differential chaos shift keying system," *IEEE Trans. Circuits Syst., II, Exp. Briefs*, vol. 63, no. 7, pp. 648-652, Jul. 2016.

[52] J. G. Proakis and M. Salehi, *Digital Communications*. New York, NY, USA: McGraw-Hill, 2007.

[53] M. Dawa, G. Kaddoum and M. Herceg, "A framework for the lower bound on the BER of DCSK systems over multi-path Nakagami-m fading channels," *IEEE Trans. Circuits Syst., II, Exp. Briefs*, vol. 67, no. 10, pp. 1859-1863, Oct. 2020.

[54] E. T. Jaynes, *Probability Theory: The Logic of Science*. Cambridge, U.K.: Cambridge Univ. Press, 2003.

[55] G. Kaddoum, P. Charge, and D. Roviras, "A generalized methodology for bit-error-rate prediction in correlation-based communication schemes using chaos," *IEEE Commun. Lett.*, vol. 13, no. 8, pp. 567-569, Aug. 2009.

[56] H. Yang, W. K. S. Tang, G. Chen and G. Jiang, "Multi-carrier chaos shift keying: System design and performance analysis," *IEEE Trans. Circuits Syst. I, Reg. Papers*, vol. 64, no. 8, pp. 2182-2194, Aug. 2017.

[57] M. K. Simon and M.-S. Alouini, *Digital Communication Over Fading Channels*, vol. 95, 2nd ed. Newark, NJ, USA: Wiley, 2005.

Xiangming Cai received the B.Sc. degree in information engineering from Guangdong University of Technology, Guangzhou, China, in 2017. He is currently pursuing the Ph.D. degree with the Department of Information and Communication Engineering, Xiamen University, Xiamen, China. His research interests include chaos-based digital communications, chaotic secure communications and their applications to wireless communications.

Weikai Xu (S'10-M'12) received the B.S. degree in electronic engineering from Three Gorges College, Chongqing, China, in 2000, the M.Sc. degree in communication and information system from the Chongqing University of Posts and Telecommunications, Chongqing, China, in 2003, and the Ph.D. degree in electronic circuit and system from the Xiamen University of China, Xiamen, China, in 2011. From 2003 to 2012, he was a Teaching Assistant, and Assistant Professor with the Department of Communication Engineering, Xiamen University. He is now an Associate Professor with the department of Information and Communication Engineering, Xiamen University. His research interests include chaotic communications, underwater acoustic communications, channel coding, cooperative communications and ultra-wideband.

Lin Wang (S'99-M'03-SM'09) received the M.Sc. degree in applied mathematics from the Kunming University of Technology, China, in 1988, and the Ph.D. degree in electronics engineering from the University of Electronic Science and Technology of China, China, in 2001. From 1984 to 1986, he was a Teaching Assistant with the Mathematics Department, Chongqing Normal University. From 1989 to 2002, he was a Teaching Assistant, a Lecturer, and then an Associate Professor in applied mathematics and communication engineering with the Chongqing University of Post and Telecommunication, China. From 1995 to 1996, he was with the Mathematics Department, University of New England, Armidale, NSW, Australia, for one year. In 2003, he was a Visiting Researcher with the Center for Chaos and Complexity Networks, Department of Electronic Engineering, City University of Hong Kong, for three months. In 2013, he was a Senior Visiting Researcher with the Department of ECE, University of California at Davis, Davis, CA, USA. From 2003 to 2012, he was a Full Professor and an Associate Dean with the School of Information Science and Engineering, Xiamen University, China. He has been a Distinguished Professor since 2012. He holds 14 patents in the field of physical layer in digital communications. He has authored over 100 journal and conference papers. His current research interests are in the area of channel coding, joint source and channel coding, chaos modulation, and their applications to wireless communication and storage systems.

Guanrong Chen (M'89-SM'92-F'97-LF'19) received the M.Sc. degree in computer science from Sun Yat-sen University, Guangzhou, China, in 1981, and the Ph.D. degree in applied mathematics from Texas A&M University, College Station, TX, USA, in 1987. He was a tenured Full Professor with The University of Houston, Houston, TX, USA. He has been a Chair Professor and the Founding Director of the Centre for Chaos and Complex Networks, City University of Hong Kong, since 2000. He is a member of the Academy of Europe and a Fellow of The World Academy of Sciences. He received the State Natural Science Award of China, in 2008, 2012, and 2016, respectively. He was awarded the 2011 Euler Gold Medal, Russia, and conferred Honorary Doctorates by the Saint Petersburg State University, Russia, in 2011, and by the University of Le Havre, Normandy, France, in 2014. He has been a Highly Cited Researcher in Engineering according to Thomson Reuters since 2009.